

Grounding the Ungrounded: A Spectral-Graph Framework for Quantifying Hallucinations in multimodal LLMs

Supratik Sarkar ^{*} ¹ and Swagatam Das [†] ²

¹Morgan Stanley

²Indian Statistical Institute (Kolkata), India

August 10, 2025

Abstract

Hallucinations in large language models (LLMs) remain a fundamental obstacle to trustworthy AI, particularly in high-stakes multimodal domains such as medicine, law, and finance. Existing evaluation techniques are largely heuristic—anchored in qualitative benchmarking or ad-hoc empirical mitigation—providing neither principled quantification nor actionable theoretical guarantees. This gap leaves a critical blind spot in understanding how hallucinations arise, propagate, and interact across modalities. We introduce the first (to our knowledge) rigorous information geometric framework in diffusion dynamics for quantifying hallucinations in multimodal LLMs (MLLMs), advancing the field from qualitative detection to mathematically grounded measurement. Our approach represents MLLM outputs as the spectral embeddings over multimodal graph Laplacians and characterizes the manifold gaps of truth vs inconsistencies as the semantic distortion, enabling the tight Rayleigh–Ritz bounds on the multimodal hallucination energy as a functional of time-dependent temperature profiles. By leveraging eigenmode decompositions in Reproducing Kernel Hilbert Space (RKHS) embeddings, our framework delivers modality-aware, theoretically interpretable metrics that capture the evolution of hallucinations across time and input prompts through temperature annealing. This work establishes a principled foundation for quantifying and bounding hallucinations, transforming them from a qualitative risk to a tractable, analyzable phenomenon.

1 Introduction

Large language models (LLMs) and their multimodal extensions (MLLMs) have demonstrated remarkable generative capabilities across diverse domains, yet their reliability remains a persistent challenge. A particularly critical failure mode is hallucination—the generation of content that is ungrounded, factually incorrect, or inconsistent with the provided input modalities. In safety-sensitive applications such as medicine, law, and finance, hallucinations can lead to severe consequences, underscoring the need for rigorous evaluation and mitigation frameworks [1, 2, 3].

Existing works have primarily addressed hallucination using heuristic or qualitative approaches. Benchmarking studies such as [1, 2, 4] provide taxonomies and evaluation datasets, while recent multimodal studies (e.g., [5]) focus on empirical detection and mitigation techniques. However, these frameworks typically lack principled, quantitative foundations, instead relying on proxy metrics, task-specific annotations, or human evaluation.

^{*}supratik.sarkar@morganstanley.com

[†]swagatam.das@isical.ac.in

From a theoretical perspective, Vempala et al. [6] demonstrate that *calibrated language models must necessarily hallucinate* under certain assumptions, revealing a fundamental trade-off between calibration and truthfulness. This result provides a compelling theoretical backdrop for understanding hallucinations as a structural property of generative models rather than a mere training artifact. Yet, while such works advance our conceptual understanding, they do not provide operational tools for quantifying hallucination in real-world systems.

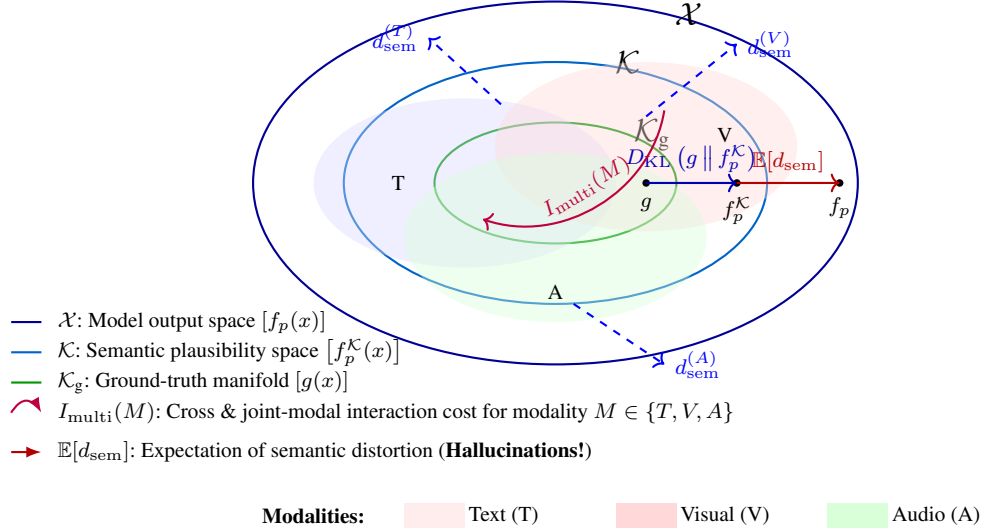


Figure 1: Multimodal nested-manifold representation of hallucination divergence and semantic distortion. Three hollow ellipses represent \mathcal{X} , \mathcal{K} , and \mathcal{K}_g with distinct borders. Shaded overlapping slices indicate modality-specific regions (Text: T , Vision: V , Audio: A), extending beyond \mathcal{K} into \mathcal{X} , capturing cross & joint-modal hallucinations where $I_{\text{multi}}(M)$ encodes what we will see in Eq. (11). Arrows represent hallucination divergence and semantic distortion penalties. The purple curved arrow represents $I_{\text{multi}}(M)$, the co-information penalty quantifying hallucinations from multimodal dependencies.

Other top-tier contributions include Jiang et al.’s NAACL-24 study examining token-level dynamics of hallucinated predictions, and Wang et al.’s EMNLP-23 Bayesian sequential framework for efficient hallucination detection [7, 8]. At ICML 2024, Han et al. introduced semantic entropy probes (SEPs) for lightweight uncertainty-based hallucination detection [9]. At ICML 2025, Park et al. proposed a latent-space steering vector (TSV) to better separate truthful and hallucinatory generations [10]. Complementary NeurIPS work on CrossCheckGPT performed universal reference-free hallucination ranking for multimodal foundation models [11].

Some recent studies have begun to incorporate structural or spectral insights into hallucination detection. For example, graph-based spectral analysis has been proposed to probe attention maps and feature representations in unimodal LLMs [12]. However, these efforts are limited to detection and classification, falling short of delivering a comprehensive framework for quantifying hallucinations, particularly in multimodal settings where interactions between modalities compound the complexity of grounding.

Despite this rich array of efforts, the field still lacks a quantitative, theory-backed, modality-aware framework that models hallucination as a measurable phenomenon rather than merely detected behavior. Most methods deliver detection or classification (binary or ranking), without providing continuous metrics, interpretable guarantees, or insight into temporal evolution across modalities.

Thus, there exists a clear methodological gap: current approaches either (i) remain heuristic and qualitative, (ii) provide only task-specific empirical diagnostics, or (iii) lack a modality-aware, theoretically

interpretable framework to quantify and bound hallucination behavior over time.

Our Contribution. We propose the first rigorous spectral framework for quantifying hallucination in MLLMs, enabling a shift from qualitative detection to quantitative, interpretable metrics. Specifically, we:

1. Frame hallucination in MLLMs as the gaps between *optimal transport* paths in generative diffusion dynamics, enabling a structural representation of grounding across modalities in Reproducing Kernel Hilbert Space (RKHS) embeddings.
2. Model the outputs as spectral embeddings over multimodal graph Laplacians, yielding the tight *Rayleigh–Ritz bounds* on the hallucination energy as a function of time-dependent temperature profiles.
3. *Empirical validation:* In addition to our theoretical contributions, we designed supporting experiments to validate our framework on both (i) synthetic and (ii) real-world datasets - Hallu-PI (unimodal, [4]) & GraphEval (multimodal, [13]) to provide initial evidence that these sandwich bounds we have theoretically derived are able to capture the practical evolution of hallucination energy under the temperature-controlled spectral graphs. Extended experiments and ablation studies are explicitly demonstrated in supplementary materials.

To illustrate our approach, Figure 1 provides a conceptual overview of how hallucination is modeled within our proposed framework. It depicts model outputs embedded as nodes in a multimodal graph Laplacian, where the grounding gaps correspond to hallucination metric motivating our quantitative treatment to control or mitigate hallucinations.

This framework advances the study of hallucinations from qualitative detection to quantitative, modality-aware, and theoretically interpretable guarantees. To our knowledge, this is the first work to provide spectral bounds on hallucination energy in MLLMs, establishing a principled foundation for future evaluation and mitigation strategies.

2 Related Work

As the challenge of LLM hallucinations being widely recognized, foundational theoretical analyses - such as Kalai & Vempala’s work in (STOC ’24) - shows that the hallucination rate of a calibrated language model is statistically lower bounded by the fraction of facts seen exactly once in the training set—a Good-Turing-style “monofact” estimate [6].

Empirical efforts dominate, with surveys and taxonomies outlining causes, detection, and mitigation strategies [1, 14]. Benchmarks like Hallu-PI stress-test LLMs under perturbed inputs [4], while GraphEval leverages viewpoint graphs and GNNs to improve robustness in idea evaluation [13].

Detection methods increasingly focus on uncertainty and structural signals: semantic-entropy probes [9], Bayesian sequential estimation [8], token-level dynamics [7], and zero-shot reasoning [15]. Sampling-based methods like SelfCheckGPT assess consistency across generations [16].

Spectral and graph-theoretic approaches extract structural cues: FactSelfCheck models outputs as knowledge graphs for fine-grained hallucination detection [17]; LapEigvals leverages attention-map Laplacian spectra [18]; and Le Merrer & Tredan study hallucinated graphs using topological distances [19]. While effective for detection, these methods stop short of quantifying hallucination dynamics in multimodal, generative settings.

However, the field still lacks a quantitative, modality-aware, generative-theoretic framework that can model hallucination as a continuous phenomenon over time and across input modalities. Our work advances beyond detection: we introduce a formally grounded spectral framework that provides tight sandwich bounds

on hallucination energy based on generative diffusion dynamics, embedding modality-interactions through spectral graph constructs and Wasserstein transport.

3 Preliminaries

We begin by establishing the mathematical foundations of our framework.

3.1 Mathematical Foundations

Let \mathcal{X} denote the measurable¹ set of all possible model outputs of a multimodal LLM, with \mathcal{F} being σ -algebra over \mathcal{X} and μ being the base measure [20]; e.g., counting measure for discrete outputs like token sequence or Lebesgue measure for continuous ones like embeddings [21]. We assume \mathcal{X} is continuously embedded in a separable reproducing kernel Hilbert space (RKHS) denoted by $(\mathcal{H}, \langle \cdot, \cdot \rangle_{\mathcal{H}})$ which is associated with a positive-definite kernel,

$$K : \mathcal{X} \times \mathcal{X} \rightarrow \mathbb{R}^+. \quad (1)$$

The kernel $K(x_1, x_2)$ encodes the semantic relationships between two distinct points or outputs x_1 and $x_2 \forall (x_1 \neq x_2) \in \mathcal{X}$; for example, through embedding-based or ontology-aware distance measures, or co-reference resolution. For a product kernel in an MLLM, refer to Eq. (10) later.

Within this $(\mathcal{X}, \mathcal{F}, \mu)$ space, there exist two kinds of “truth” (the idea imported from [6]):

- (i) The semantic factoid space \mathcal{K} which encompasses all semantically valid and coherent outputs that include empirically plausible facts, contextually appropriate completions, and domain-consistent inferences aligned with the prompt and background knowledge - importantly, elements of \mathcal{K} need not be verifiable, but they remain semantically valid within the modeled domain.
- (ii) The semantic ground-truth manifold \mathcal{K}_g , as a stricter subregion of \mathcal{K} , which consists of outputs only verifiably correct or true facts that include factual assertions supported by empirical evidence or directly observed information — elements of \mathcal{K}_g can be properly referred to as grounded in reality.

Thus, the semantic plausibility and ground-truth are embodied as

$$\mathcal{K}_g \subseteq \mathcal{K} \subset \mathcal{X}. \quad (2)$$

For a given prompt $p \in \mathcal{P}$, each output denoted by $x \in \mathcal{X}$ contributes to hallucination iff

$$x \in \mathcal{X} \setminus \mathcal{K}. \quad (3)$$

Note: $x \in \mathcal{K} \setminus \mathcal{K}_g$ is a non-grounded output, but still semantically plausible and strictly not hallucination.

3.2 Modeling the LLM outputs

The LLM outputs can be characterized by a conditional probability distribution $f_p(x)$ that denotes the likelihood of generating output x given a prompt p :

$$f_p : \mathcal{X} \rightarrow [0, \infty), \quad f_p \in L^1(\mathcal{X}, \mathcal{F}, \mu) \cap \mathcal{H}, \quad x \mapsto f_p(x), \quad (4)$$

which ensure $\int_{\mathcal{X}} f_p(x) d\mu(x) = 1$.

¹Footnotes are added in the exact chronological order, starting from this one itself, later in the Appendix A (Technical Notes or Extended Comments) of this paper.

Let f_p^K denote the restricted distribution on the semantic plausibility space \mathcal{K} :

$$f_p^K(x) := \frac{\mathbf{1}_{\{x \in \mathcal{K}\}} f_p(x)}{\int_{\mathcal{K}} f_p(x') d\mu(x')} \equiv \frac{\mathbf{1}_{\{x \in \mathcal{K}\}} f_p(x)}{\mathbb{P}_{f_p}(\mathcal{K})}, \quad \text{where, } \mathbf{1}_{\{x \in \mathcal{K}\}} = \begin{cases} 1 & \text{if } x \in \mathcal{K}, \\ 0 & \text{otherwise.} \end{cases} \quad (5)$$

Here, $\int_{\mathcal{K}} f_p(x') d\mu(x') = \mathbb{P}_{f_p}(\mathcal{K})$ is a constant term acts as a normalization in the restricted distribution.

Subsequently, let's also assume g denotes the restricted distribution on the ground-truth manifold \mathcal{K}_g . Unlike f_p or f_p^K , g is the gold reference which is not model-induced and hence, may not share support with f_p except inside \mathcal{K}_g and it's truly independent of prompts in the generative sense (but conditioned on the same prompt contextually). Thus, we do not assume any parametric form for the ground-truth distribution g and rather treat it as an abstract measure over \mathcal{K}_g :

$$\text{supp}(g) \subseteq \mathcal{K}_g, \quad g : \mathcal{K}_g \rightarrow [0, \infty), \quad g \in L^1(\mathcal{K}_g, \mathcal{F}|_{\mathcal{K}_g}, \nu), \quad (6)$$

which ensure $\int_{\mathcal{K}_g} g(x) d\nu(x) = 1$ with notations used in consistency with Eq. (4) and ν playing the same role of μ , but not necessarily equal to μ . The absence of an exact analytical expression of $g(x)$ limits the direct interpretability, but provides a flexible framework for comparing the model outputs to the ground-truth via the functional and spectral metrics.

4 Theoretical Analysis

In this section, we present a rigorous theoretical formulation that we have developed to address the problem of hallucination quantification in MLLMs, identifying semantic distortions as the root metric for hallucinations through a series of theorems, lemma(s), corollaries, and accompanying proof sketches.

4.1 Semantic Distortion

We establish the following theorem to set the stepping stone.

Theorem 1 (KL Decomposition with Ground-Truth Reference). *The deviation of the model output f_p w.r.t the ground-truth g can be measured by Kullback–Leiblere (KL) divergence² that admits a straightforward decomposition as below:*

$$D_{\text{KL}}(g \parallel f_p) = D_{\text{KL}}(g \parallel f_p^K) + \log[\mathbb{P}_{f_p}(\mathcal{K})]. \quad (7)$$

Proof Sketch.

See Appendix B.1 for the full derivation. The key idea is to start decomposing the KL divergence between the most “distant” distributions g and f_p w.r.t the base measure μ of the entire space $(\mathcal{X}, \mathcal{F}, \mu)$, keeping it consistent with the theory of information geometry [22]. By definition (see Section A.2), we have:

$$D_{\text{KL}}(g \parallel f_p) = \int_{\mathcal{K}_g} g(x) \log \frac{g(x)}{f_p(x)} d\mu(x) = D_{\text{KL}}(g \parallel f_p^K) + \int_{\mathcal{K}_g} g(x) \log \left[\frac{\mathbf{1}_{\{x \in \mathcal{K}\}}}{\mathbb{P}_{f_p}(\mathcal{K})} \right] d\mu(x), \quad (8)$$

with substitution from Eq. (5). In this context, we identify $d_{\text{sem}}(x; \mathcal{K}, \mathcal{X})$ as the semantic distortion term giving rise to hallucinations and its expectation under the ground truth distribution g :

$$d_{\text{sem}}(x; \mathcal{K}, \mathcal{X}) = \log \frac{f_p^K(x)}{f_p(x)}, \quad \text{i.e., } \mathbb{E}_{x \sim g}[d_{\text{sem}}(x; \mathcal{K}, \mathcal{X})] = \int_{\mathcal{K}_g} g(x) \log \frac{f_p^K(x)}{f_p(x)} d\mu(x). \quad (9)$$

Eq. (8) proves the stated identity. \square

Remark 1. The divergence $D_{\text{KL}}(g \parallel f_p)$ represents the extra coding cost (in nats) to describe the “true”, grounded distribution g using the model’s output distribution f_p while $\mathbb{E}_g[d_{\text{sem}}]$ is the hallucination penalty for an output $x : f_p^{\mathcal{K}} \rightarrow f_p$. It is the metric we are after to quantify hallucinations in language models. The above decomposition (Eq. (7)) separates two interpretable components³ along with by a sanity check $\mathbb{P}_{f_p}(\mathcal{K} = \mathcal{X}) = 1$ meaning $\mathbb{E}_g[d_{\text{sem}}] = 0$, as expected.

In multimodal settings, this decomposition provides actionable insights: we can isolate hallucination contributions to each modality and their interactions, guiding targeted mitigation strategies (e.g., modality-specific calibration or cross-modal consistency constraints).

4.2 Extension to Multi-modal Grounding

The intuition behind this setting is: in image-grounded or dialogue models, semantic grounding depends on multiple modalities — e.g., text, image or video, dialog or audio-history etc. and the RKHS is then extended to a multi-modal product kernel space.

In multi-modal settings, where the LLM outputs involve textual (T), visual (V), audio (A) modalities, we define a joint output space (\mathcal{X}) embedded into a composite RKHS (\mathcal{H}) equipped with a product kernel (K) between two distinct points (i.e., outputs) $\forall (x_1 \neq x_2) \in \mathcal{X}$ as

$$\begin{aligned} \mathcal{X} : \times_M \mathcal{X}_M, \quad x &= (x^{(M)})_{x^{(M)} \in \mathcal{X}_M}, \quad \mathcal{H} := \otimes_M \mathcal{H}_M, \\ K(x_1, x_2) &= \prod_M K_M(x_1^{(M)}, x_2^{(M)}), \quad \mathcal{P} : \times_M \mathcal{P}_M, \\ p &= (p^{(M)})_{p^{(M)} \in \mathcal{P}_M}, \quad \forall M \in \mathcal{M} := \{T, V, A\}. \end{aligned} \quad (10)$$

Here, we have considered three different kinds of probable prompts (text, visual and audio) in a composite prompt space $\mathcal{P} : \times_M \mathcal{P}_M$ for the sake of completeness. However, in the following calculation, we restrict ourselves only to the notion of p without any loss of generality. The above Eq. (10) employs a compact mathematical notation⁴ to represent multimodal components succinctly.

4.3 Formulations to Hallucination Energy

To begin with, we are after a fruitful formulation of f_p that connects the model output distribution to an underlying energy landscape $\mathcal{E}(x, p)$, enabling (i) interpretability of mode concentration, (ii) incorporation of temperature-driven exploration, and (iii) spectral graph-based analysis of energy propagation.

For kernel K_M , let $\Phi_M : \mathcal{X}_M \rightarrow \mathcal{H}_M$ be its feature map (using the results of Moore–Aronszajn theorem [23]) for each modality $M \in \mathcal{M}$. Feature maps can be viewed as operators⁵ that embed data points into a high-dimensional (possibly infinite-dimensional) Hilbert space.

The total energy functional $\mathcal{E}(x, p)$ can be decomposed into intra-modal, pairwise cross-modal, and joint multimodal interactions. This decomposition allows us to localize the sources of hallucination within and across modalities. This structure not only reveals which modality interactions contribute most to semantic drift but also enables deriving tight spectral bounds (via Rayleigh–Ritz, see Eq. (68) in Appendix C for more details) on hallucination energy, which would be impossible under a monolithic energy formulation.

We have:

$$\mathcal{E}(x, p) = \sum_{M \in \mathcal{M}} \mathcal{E}_M(x^{(M)}, p) + \sum_{\substack{M, M' \in \mathcal{M} \\ M \neq M'}} \mathcal{E}_{MM'}(x^{(M)}, x^{(M')}, p) + \mathcal{E}_{\mathcal{M}}(x, p). \quad (11)$$

Here, (i) \mathcal{E}_M encodes the intra-modal contributions being the only term that survives if there is zero overlap between modalities, (ii) $\mathcal{E}_{MM'}$ captures the pairwise cross-modal contributions while (iii) $\mathcal{E}_{\mathcal{M}}$ being the joint

contribution of all three modalities combined. Evidently, (i) and (ii) constitute a matrix of order 3 where the diagonal entries are \mathcal{E}_M and off-diagonal entries are $\mathcal{E}_{MM'}$. In our current formulation, (iii) is a single term, however, if there exist > 3 modalities (say, physiological signals like EEG or ECG, haptics like touch or force sensors etc.), then this joint term $\mathcal{E}_{\mathcal{M}}$ becomes a tensor of higher rank. Refer to Eqs. (20) & (65) for the similar construction in terms of Laplacians.

Theorem 2 (Multimodal Energy-based Hallucination Formalism). *Let the output distribution f_p of an MLLM with modalities ($M \in \mathcal{M} := \{T, V, A\}$), for a given prompt $p \in \mathcal{P}$, assume the Boltzmann form:*

$$f_p(x) = \frac{1}{Z(p, \mathcal{T}_t)} \exp\left(-\frac{\mathcal{E}(x, p)}{\mathcal{T}_t}\right), \quad (12)$$

where $\mathcal{T}_t \geq 0$ is a temperature parameter dependent on time ($t \geq 0$), and

$$Z(p, \mathcal{T}_t) = \int_{\mathcal{X}} \exp\left(-\frac{\mathcal{E}(x, p)}{\mathcal{T}_t}\right) d\mu(x) \quad (13)$$

is the normalizing partition function ensuring $f_p \in L^1(\mathcal{X}, \mathcal{F}, \mu)$ as per Eq. (4). Then each term on r.h.s of Eq. (11) for $\mathcal{E}(x, p)$ would be given by:

$$\mathcal{E}_M(x^{(M)}, p) = \|\Phi_M(x^{(M)}) - \Phi_M(p)\|_{\mathcal{H}_M}^2, \quad (14a)$$

$$\mathcal{E}_{MM'}(x^{(M)}, x^{(M')}, p) = -\left\langle \Phi_M(x^{(M)}), \Phi_{M'}(x^{(M')}) \right\rangle_{\mathcal{H}_{MM'}} + \underbrace{\left\langle \Phi_M(p), \Phi_{M'}(p) \right\rangle_{\mathcal{H}_{MM'}}}_{\Psi_{MM'}(p)}, \quad (14b)$$

$$\mathcal{E}_{\mathcal{M}}(x, p) = -\left\langle \bigotimes_{M \in \mathcal{M}} \Phi_M(x^{(M)}), \underbrace{\bigotimes_{M \in \mathcal{M}} \Phi_M(p)}_{\Theta(p)} \right\rangle, \quad (14c)$$

where $\Psi_{MM'}(p)$ and $\Theta(p)$ are prompt-conditioned bias terms modulating cross- and joint-modal interactions respectively.

Proof Sketch.

See Appendix B.2 for the full derivation. The key idea is, in this setting, the interaction energy acts as a semantic dissimilarity between any two objects (be it inputs and/or outputs) in the RKHS \mathcal{H}_M induced by the chosen kernel K_M .

Specifically, the intra-modal terms (Eq. (14a)) measure the squared Hilbert-space norm between the feature maps of the generated object (i.e., x) and that of the given prompt (i.e., p) and

$$\text{by construction: } \|\Phi_M(x^{(M)}) - \Phi_M(p)\|_{\mathcal{H}_M}^2.$$

Similarly, substituting the cross-modal terms (Eq. (14b)) and joint-modal term (Eq. (14c)) into the Boltzmann form (Eq. (12)) yields the full multimodal energy-based formalism. \square

Lemma 1 (Unimodal Sanity Check). *If $|\mathcal{M}| = 1$, then Eq. (11) survives only with the first term on r.h.s which is a purely intra-modal contribution.*

Proof. If $|\mathcal{M}| = 1$, then no pairs (M, M') exist, so $\sum_{M \neq M'} \mathcal{E}_{MM'} = 0$, and no triple-interaction: $\mathcal{E}_{\mathcal{M}} = 0$. So only Eq. (14a) survives in Eq. (11), proving the claim. \square

Corollary 1 (Free Energy Gap). *Combining Theorem 1 with Eqs. (12) & (13), the hallucinations in an MLLM can be quantified through the Boltzmann partition functions of the model output distribution:*

$$\begin{aligned} d_{sem} &= D_{\text{KL}}(g \parallel f_p) - D_{\text{KL}}(g \parallel f_p^{\mathcal{K}}) \\ &= \log \left[\frac{Z(p, \mathcal{T}_t)}{Z_{\mathcal{K}}(p, \mathcal{T}_t)} \right] \equiv \frac{1}{\mathcal{T}_t} \Delta_{\mathcal{K} \rightarrow \mathcal{X}}(\text{free energy}). \end{aligned} \quad (15)$$

See Appendix B.3 for the detailed proof. \square

Corollary 2 (Hallucination Energy). *In line with Theorem 1, we identify the total hallucination energy in a multimodal LLM as:*

$$\mathcal{E}_{\text{hall}}^{\text{multi}}(x, p, \cdot) = \mathcal{E}(x, p, \cdot) - \mathcal{E}_{\mathcal{K}}(x, p, \cdot), \quad (16)$$

where $\mathcal{E}(x, p, \cdot)$ is the full energy term at \mathcal{X} (using Eq. (11)) and $\mathcal{E}_{\mathcal{K}}(x, p, \cdot)$ is the same restricted at \mathcal{K} .

Proof. This particular Corollary does not require any explicit proof as this is merely an identification done by the authors in line with the results obtained in Theorem 1. \square

Example (Image–Caption Pair). Let’s consider an MLLM generating a caption for an image. Let \mathcal{X} be the space of all captions, with $\mathcal{K} \subseteq \mathcal{X}$ denoting those grounded in the image (e.g., “A cat on a sofa”), while f_p may also assign mass outside \mathcal{K} to hallucinated captions (e.g., “A dog playing with a ball”). The hallucination divergence $D_{\text{KL}}(g \parallel f_p)$ quantifies this deviation.

The multimodal graph Laplacian $\mathcal{L}_{\mathcal{T}_t}^{\text{multi}}$ encodes relationships between image features and caption tokens with edge weights $W_{\mathcal{T}_t}(i, j)$ modulated by a time-varying temperature \mathcal{T}_t . Its spectral decomposition reveals how hallucination energy distributes across modes (e.g., textual vs. cross-modal misalignments).

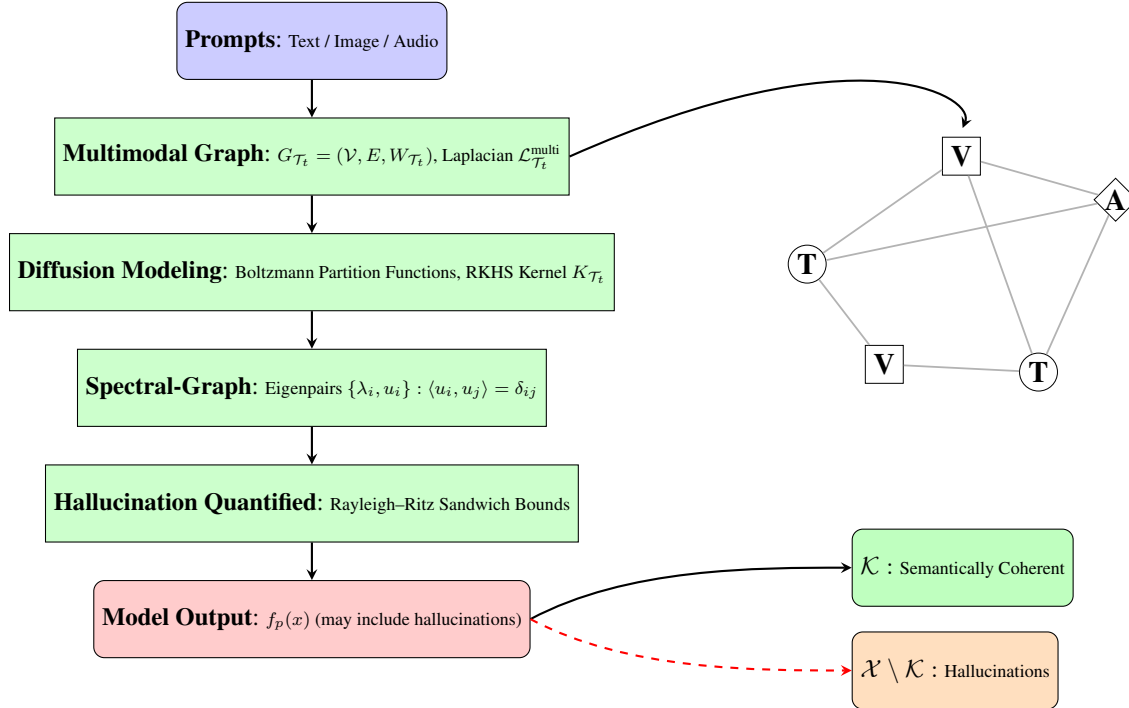


Figure 2: Pipeline for hallucination quantification in MLLMs.

5 Main Results: Proposed Framework

In this section, we present our primary theoretical contributions to build a systematic framework (Figure 2). We start with reformulating the multimodal hallucination energy $\mathcal{E}_{\text{hall}}^{\text{multi}}$, as noted in Eq. (16), using the spectral-graph theory [24]. This allows us to connect the Boltzmann partition function of the model outputs to the eigenmodes of a multimodal semantic graph Laplacian (to be identified later), thereby providing a principled way to bound hallucination energy.

5.1 Spectral-Graph Propagation

Let a time-evolving temperature-dependent semantic knowledge graph (multimodal) at an instant t be denoted by

$$G_{\mathcal{T}_t} = (\mathcal{V}, E, W_{\mathcal{T}_t}), \quad \mathcal{V} \subseteq \mathbb{N}, \quad E \subseteq \mathcal{V} \times \mathcal{V}, \quad W_{\mathcal{T}_t} \in \mathbb{R}^{|\mathcal{V}| \times |\mathcal{V}|}; \quad \forall t \in \mathbb{R}^+, \quad (17a)$$

$$\mathcal{T}_t \begin{cases} : \mathcal{V} \rightarrow \mathbb{R}^+ & (\text{if node-wise, i.e., a local function}) \\ \in \mathbb{R}^+ & (\text{if const., i.e., a global scalar}) \end{cases} \quad (17b)$$

where \mathcal{V} is the set of nodes, E is the set of edges, and $W_{\mathcal{T}_t}$ is a temperature-modulated weighted adjacency matrix. Here, each node represents a semantic unit (e.g., concepts, tokens, ideas), and edges represent the semantic similarity.

Now the temperature \mathcal{T}_t dynamically modulates the graph edge connectivity and semantic drift. This time-varying function captures the semantic evolution or uncertainty drift across the graph nodes as knowledge updates over time. It modulates the semantic smoothness - meaning lower values produce sharper (localized) edges in the graph, while higher values induce more “noise”.

The weighted adjacency matrix $W_{\mathcal{T}_t}$ is introduced to assign different weights to all the edges, indexed by E . See Appendix A.6 for its full expression.

Note: For graph representations, in Eqs. (17), we drop the explicit superscript (M) for different modalities as $G_{\mathcal{T}_t}$ is already multimodal. It is an integrated representation where the nodes (i, \dots, j, \dots) represent multiple modalities in one combined structure. In this case, the modality information is encoded within the nodes or edge weights, not in separate graphs.

5.2 Diffusion Kernel and Feature Map

In the current prescription of time-dependent temperature, the RKHS \mathcal{H} is associated with a positive-definite multimodal diffusion kernel (in connection with Eq. (10)) as:

$$K_{\mathcal{T}_t} := \exp\left(-\tau \mathcal{L}_{\mathcal{T}_t}^{\text{multi}}\right), \quad (18)$$

where $\tau \in \mathbb{R}^+$ is a diffusion time-scale and $\mathcal{L}_{\mathcal{T}_t}^{\text{multi}}$ is a graph Laplacian. See the next subsection 5.3 for more details.

By Mercer’s theorem [25], see Appendix A.7 for details, $K_{\mathcal{T}_t}$ induces an RKHS \mathcal{H} with feature map $\Phi : \mathcal{V} \rightarrow \mathcal{H}$ satisfying:

$$\left\langle \Phi(i), \Phi(j) \right\rangle_{\mathcal{H}} = K_{\mathcal{T}_t}(i, j) \quad \forall (i, j) \in \mathcal{V}. \quad (19)$$

Thus, the feature maps Φ_M , used in our energy functional (see Eq. (14)), are nothing but the embeddings of graph nodes (say i, \dots, j, \dots) into \mathcal{H} induced by the multimodal diffusion kernel $K_{\mathcal{T}_t}(i, j)$.

5.3 Multimodal Laplacian with All Interaction Terms

Now we define the multimodal Laplacian to incorporate intra-, cross-, and joint-modal interactions across modalities (in line with Eq. (11)):

$$\mathcal{L}_{\mathcal{T}_t}^{\text{multi}} = \sum_{M \in \mathcal{M}} \alpha_M \mathcal{L}_{\mathcal{T}_t}^{(M)} + \sum_{\substack{M \neq M' \\ M, M' \in \mathcal{M}}} \beta_{MM'} \mathcal{L}_{\mathcal{T}_t}^{(MM')} + \gamma_{\mathcal{M}} \mathcal{L}_{\mathcal{T}_t}^{(\mathcal{M})}, \quad (20)$$

with $\alpha_M, \beta_{MM'}, \gamma_{\mathcal{M}} \in \mathbb{R}_{\geq 0}$; where, (i) $\mathcal{L}_{\mathcal{T}_t}^{(M)}$ denotes the intra-modal Laplacian for each M , (ii) $\mathcal{L}_{\mathcal{T}_t}^{(MM')}$ represents pairwise cross-modal Laplacians capturing interactions between any two modalities M and M' , and (iii) $\mathcal{L}_{\mathcal{T}_t}^{(\mathcal{M})}$ is a joint-modal Laplacian representing higher-order interactions across all modalities \mathcal{M} .

The coefficients $\alpha_M, \beta_{MM'}$, and $\gamma_{\mathcal{M}}$ are non-negative interaction weights that can be tuned to adjust the relative importance of intra-, cross-, and joint-modal contributions respectively. We consider $\beta_{MM'} = \beta_{M'M}$ to impose symmetricity without any loss of generality.

5.4 Spectral Decomposition of Multimodal Laplacian

We need a principled way to disentangle and analyze mode-specific, cross-modal and joint-modal interactions, enabling us to systematically study how hallucination energy propagates across modalities in an MLLM. Let $\left\{(\lambda_i(t), u_i(t))\right\}_{i=1}^{|\mathcal{V}|}$ denote the eigenpairs of multimodal Laplacian $\mathcal{L}_{\mathcal{T}_t}^{\text{multi}}$ that acts as a spectral projector:

$$\mathcal{L}_{\mathcal{T}_t}^{\text{multi}} = U \Lambda U^\top = \sum_{i=1}^{|\mathcal{V}|} \lambda_i(t) \underbrace{\left\langle u_i(t), \cdot \right\rangle u_i(t)}_{u_i(t) u_i(t)^\top}, \quad (21)$$

where orthonormality holds true: $\left\langle u_i(t), u_j(t) \right\rangle = \delta_{ij}$ with δ_{ij} being the Kronecker delta and $\langle u_i, \cdot \rangle$ denotes the standard Euclidean inner product (or a graph inner product if we weight by a measure). See Appendix A.8 for explicit details on the eigenpairs.

5.5 Feature Map and Energy Functional

Any feature embedding $\Phi(x, t)$, according to Eq. (19), can be expressed in this time-evolving eigenbasis as:

$$\Phi(x, t) = \sum_{i=1}^{|\mathcal{V}|} e^{-\frac{\tau \lambda_i(t)}{2}} \left\langle u_i(t), \delta_x \right\rangle u_i(t), \quad (22)$$

where δ_x is the Dirac delta function (or Kronecker delta, in the discrete case) at node output x . Consequently, in line with Eq. (14a), the squared RKHS distance becomes:

$$\|\Phi(x, t) - \Phi(p, t)\|_{\mathcal{H}}^2 = \sum_{i=1}^{|\mathcal{V}|} e^{-\tau \lambda_i(t)} \left| \left\langle u_i(t), (\delta_x - \delta_p) \right\rangle \right|^2. \quad (23)$$

Substituting (23) into the intra-, cross-, and joint-modal energy definitions, the full multimodal energy

as expressed in Eqs. (14), at temperature \mathcal{T}_t , becomes:

$$\begin{aligned} \mathcal{E}(x, p, \mathcal{T}_t) &= \sum_{M \in \mathcal{M}} \sum_{i=1}^{|\mathcal{V}|} \alpha_M(\dots) + \sum_{\substack{M \neq M' \\ M, M' \in \mathcal{M}}} \sum_{i=1}^{|\mathcal{V}|} \beta_{MM'}(\dots) + \sum_{i=1}^{|\mathcal{V}|} \gamma(\dots) \end{aligned} \quad (24)$$

The full expression of $\mathcal{E}(x, p, \mathcal{T}_t)$ would be found in Appendix A.9 (Eq. (34)).

Why time-varying eigenpairs? - The semantic Laplacian evolves as the temperature \mathcal{T}_t changes, reflecting the diffusion-like adaptation of the semantic space. Refer to Appendix A.10 for some extended comments on the justification and motivation behind the adoption of this framework.

5.6 Hallucination Energy and Time-Decay

The Boltzmann partition functions $Z_\Omega(p, \mathcal{T}_t) : \Omega \in \{\mathcal{X}, \mathcal{K}\}$ become two similar functions, just integrated over two different manifolds: \mathcal{X} and its restricted counterpart \mathcal{K} , but now with $\mathcal{E}(x, p, \mathcal{T}_t)$ in hand from Eq. (24).

After some rigorous derivation as detailed in the Appendix C.2, the semantic distortion expressed through Eq. (15) finally reduces to:

$$\begin{aligned} d_{\text{sem}}(t) &= -\log(\det \mathcal{C}_t), \\ \text{where, } \mathcal{C}_t &:= \text{diag} \left(\text{erf} \left(c_i \sqrt{\frac{\eta_i(t)}{\mathcal{T}_t}} \right) \right)_{i=1}^{|\mathcal{V}|}. \end{aligned} \quad (25)$$

All the new terms introduced in Eq. (25), up until Eq. (28), with relevant explanations are accurately captured in the Appendices C.2 & C.3.

Using Eq. (16), we define the hallucination energy, with $\Delta\phi_i(t) = \langle u_i(t), (\delta_x - \delta_p) \rangle$, as:

$$\mathcal{E}_{\text{hall}}^{\text{multi}}(x, p, \mathcal{T}_t) := \sum_{i \in \mathcal{X} \setminus \mathcal{K}} e^{-\tau \lambda_i(t)} |\Delta\phi_i(t)|^2, \quad (26)$$

which indicates the tight Rayleigh–Ritz sandwich bounds on its evolution under time-varying temperature profiles (details in Appendix C.3 and aligned with Eq. (70)) as:

$$\lambda_{\min} \leq \frac{v^\top A v}{v^\top v} \leq \lambda_{\max}. \quad (27)$$

Time-dependence: As $\tau \rightarrow \infty$ (or equivalently as t increases), the exponential term $e^{-\tau \lambda_i(t)}$ decays, and the evolving spectrum $\lambda_i(t)$ drives high-frequency modes to decay faster. Thus:

$$\frac{d}{d\tau} \mathcal{E}_{\text{hall}}^{\text{multi}} \leq 0, \quad (28)$$

showing that diffusion over time suppresses unstable semantic modes, reducing hallucinations dynamically.

6 Experiments

We implemented some simulation-based experiments in two complementary setups: (i) synthetic graph-based simulations in RKHS and (ii) Hallu-PI [4]) & GraphEval [13] as real-world benchmarks. It indicates the validations of how temperature annealing ($\mathcal{T}_t \uparrow$ or \downarrow) shifts the hallucination energy toward either high-frequency modes (but $\not\propto \lambda_{\max}$) resulting in inconsistent outputs or rather controlling it (but $\not\propto \lambda_{\min}$) respectively. Comprehensive experimental results, including comparisons across architectures and parameter regimes, can be found in Appendix D.

7 Conclusion and Future Work

Our proposed framework has enabled: (i) a closed-form KL-based decomposition of semantic distortion (Theorem 1, Eq. (25)) as the hallucination metric; (ii) a structured breakdown of hallucination energy into multimodal components (Theorem 2, Eq. (24)); and (iii) the lower & upper bounds on the multimodal hallucinations as a function of time-varying temperature (Eq. (27)), supplemented by successive experimental validations (Appendix D).

As per Eqs. (25) and (27),

- Each eigenmode contributes a term depending on $\eta_i(t)$, which aggregates intra-, cross-, and joint-modal spectral weights.
- As $\mathcal{T}_t \downarrow 0$ (low temperature), the argument of $\text{erf}(\cdot)$ grows, driving $\text{erf} \rightarrow 1$ and thus reducing $d_{\text{sem}}(t)$: hallucinations are suppressed.
- Higher $\lambda_i(t)$ (high-frequency modes) contribute more strongly to semantic distortion at elevated temperatures ($d_{\text{sem}}(t)$ explicitly expressed in terms of $\eta_i(t)$), linking hallucination energy to spectral diffusion modes.

Future Work. Future work can include extending our spectral decomposition to dynamic streaming graphs. An important direction is tuning the hypergraph Laplacian coefficients - in conjunction with LLM hyperparameters (e.g., temperature, top- p), enabling co-optimization on real datasets for balanced semantic propagation and hallucination control.

Acknowledgments

SS gratefully acknowledges the organizational leadership support for AI research from both local and functional spaces: *Arijit Das* (Executive Director, Morgan Stanley) and *Sudha Sukumaran Kamonjoh* (Managing Director, Morgan Stanley) respectively. SS also extends sincere thanks to *Debanjan Dutta* (Indian Statistical Institute, Kolkata) for numerous insightful academic discussions that helped shape the trajectory of this work, *Arindam Khan* (Indian Institute of Science, Bengaluru) for his initial guidance in theoretical computer science, and *Subrata Mitra* (Adobe Research) for his valuable advice on prospective research directions, particularly in the field of LLMs.

References

- [1] Ziwei Ji, Nayeon Lee, Rita Frieske, Tiezheng Yu, Dan Su, Yan Xu, Etsuko Ishii, Yejin Bang, Andrea Madotto, and Pascale Fung. Survey of hallucination in natural language generation. *ACM Computing Surveys*, 55(12):1–38, 2023.
- [2] Justin Maynez, Shashi Narayan, Bernd Bohnet, and Ryan McDonald. On faithfulness and factuality in abstractive summarization. In *Proceedings of the Annual Meeting of the Association for Computational Linguistics (ACL)*, pages 1906–1919, 2020.
- [3] Sébastien Bubeck, Varsha Chandrasekaran, Ran Eldan, Johannes Gehrke, Eric Horvitz, Ece Kamar, Percy Lee, Yu Li, Scott Lundberg, Harsha Nori, et al. Sparks of artificial general intelligence: Early experiments with gpt-4. Technical report, arXiv, 2023. arXiv preprint arXiv:2303.12712.

- [4] Peng Ding, X. Hu, H. Li, X. Chen, and H. Ji. Hallu-pi: Benchmarking hallucinations under perturbed inputs for large language models. In *ICLR*, 2024.
- [5] T. Bai, Y. Zhang, X. Lin, Q. Sun, and C. Wu. Multimodal hallucinations: A survey of causes, metrics, and mitigation. Technical report, arXiv, 2024. arXiv:2404.18930.
- [6] Adam Tauman Kalai and Santosh S. Vempala. Calibrated language models must hallucinate. In *Proceedings of the 56th Annual ACM Symposium on Theory of Computing (STOC)*, pages 160–171, 2024.
- [7] C. Jiang, B. Qi, X. Hong, D. Fu, Y. Cheng, F. Meng, M. Yu, B. Zhou, and J. Zhou. On large language models’ hallucination with regard to known facts. In *NAACL*, 2024.
- [8] X. Wang, Y. Yan, L. Huang, X. Zheng, and X. Huang. Hallucination detection for generative large language models by bayesian sequential estimation. In *EMNLP*, pages 15361–15371, 2023.
- [9] J. Han, J. Kossen, M. Razzak, L. Schut, S. Malik, and Y. Gal. Semantic entropy probes: Robust and cheap hallucination detection in large language models. In *ICML Workshop on Foundation Models in the Wild*, 2024.
- [10] S. Park, X. Du, M.-H. Yeh, H. Wang, and S. Li. Steer llm latents for hallucination detection. Technical report, ICML Poster, 2025.
- [11] G. Sun, P. Manakul, A. Liusie, K. Pipatanakul, C. Zhang, P. Woodland, and M. Gales. Crosscheckgpt: Universal hallucination ranking for multimodal foundation models. In *NeurIPS Workshop on Next Gen Multimodal Models*, 2024.
- [12] J. Xie, C. Zhang, and M. Li. Spectral characterization of hallucination in large language models. Technical report, arXiv, 2025. arXiv:2502.17598.
- [13] Tao Feng, Yihang Sun, and Jiaxuan You. Grapheval: A lightweight graph-based llm framework for idea evaluation. *arXiv preprint arXiv:2503.12600*, 2025.
- [14] V. Rawte, S. Chakraborty, A. Pathak, A. Sarkar, S. M. T. I. Tonmoy, A. Chadha, A. Sheth, and A. Das. The troubling emergence of hallucination in large language models: An extensive definition, quantification, and prescriptive remediations. Technical report, 2023.
- [15] Seongmin Lee, Hsiang Hsu, and Chun-Fu Chen. Llm hallucination reasoning with zero-shot knowledge test. *arXiv preprint arXiv:2411.09689*, 2024.
- [16] Potsawee Manakul, Adian Liusie, and Mark J. F. Gales. Selfcheckgpt: Zero-resource black-box hallucination detection for generative large language models. In *Proceedings of EMNLP*, 2023.
- [17] Albert Sawczyn, Jakub Binkowski, Denis Janiak, Bogdan Gabrys, and Tomasz Kajdanowicz. Fact-selfcheck: Fact-level black-box hallucination detection for llms. *arXiv preprint arXiv:2503.17229*, 2025.
- [18] Jakub Binkowski, Denis Janiak, Albert Sawczyn, Bogdan Gabrys, and Tomasz Kajdanowicz. Spectral characterization of hallucination in large language models. *arXiv preprint arXiv:2502.17598*, 2025.
- [19] Eric Le Merrer and Gilles Trédan. Llms hallucinate graphs too: A structural perspective. *arXiv preprint arXiv:2409.00159*, 2024.

- [20] Terence Tao. *An Introduction to Measure Theory*, volume 126 of *Graduate Studies in Mathematics*. American Mathematical Society, 2011. Covers sigma-algebras, outer measures, completeness, and constructions of measure.
- [21] Robert G. Bartle. *The Elements of Integration and Lebesgue Measure*. Wiley-Interscience, corrected reprint of the 1st ed. (1966) edition, 1995. Introduction emphasizing Lebesgue measure on \mathbb{R}^n with clarity and examples.
- [22] William Cook. A hierarchical decomposition of kullback–leibler divergence: Disentangling marginal mismatches from statistical dependencies. *arXiv preprint arXiv:2504.09029*, 2025.
- [23] Nachman Aronszajn. *Theory of Reproducing Kernels*, volume 68. 1950.
- [24] Fan R. K. Chung. *Spectral Graph Theory*, volume 92 of *CBMS Regional Conference Series in Mathematics*. American Mathematical Society, Providence, RI, 1997.
- [25] James Mercer. Functions of positive and negative type, and their connection with the theory of integral equations. *Philosophical Transactions of the Royal Society A*, 209:415–446, 1909.
- [26] Dengyong Zhou, Jiayuan Huang, and Bernhard Schölkopf. Learning with hypergraphs: Clustering, classification, and embedding. *Advances in Neural Information Processing Systems*, 19:1601–1608, 2006.
- [27] Gerald B. Folland. *Real Analysis: Modern Techniques and Their Applications*. Wiley, 2nd edition, 1999.
- [28] Yasha Ektefaie et al. Multimodal learning with graphs. *Nature Machine Intelligence*, 2023. Describes how graph-based AI methods integrate multiple modalities via modality-aware adjacency structures.
- [29] Ciyuan Peng, Jiayuan He, and Feng Xia. Learning on multimodal graphs: A survey. *arXiv preprint arXiv:2402.05322*, 2024. Available at arXiv:2402.05322v1.
- [30] Zhuo Chen, Yichi Zhang, Yin Fang, Yuxia Geng, Lingbing Guo, Xiang Chen, Qian Li, Wen Zhang, Jiaoyan Chen, Yushan Zhu, Jiaqi Li, Xiaoze Liu, Jeff Z. Pan, Ningyu Zhang, and Huajun Chen. Knowledge graphs for multi-modal learning: Survey and perspective. *Information Fusion*, 121:103124, 2025.
- [31] Walther Ritz. Über eine neue methode zur lösung gewisser variationsprobleme der mathematischen physik. *Journal für die Reine und Angewandte Mathematik*, 135:1–61, 1909. Original presentation of the Rayleigh–Ritz variational method.

Appendix

In this section, we provide elaboration on footnotes, extended derivations of our Theorems, some supplementary mathematical results, and details of experimental validation.

A Technical Notes and Extended Comments

Here, we provide elaboration on footnotes/ some extended explanations.

A.1 Measurable Sets and σ -algebra

Any mathematical set can be equipped with a σ -algebra to form a measurable space, say, \mathcal{X} . The common choices are: (i) the power set if \mathcal{X} is countable/ finite, (ii) the Borel σ -algebra if \mathcal{X} is a topological space (e.g., continuous embeddings), (iii) Product σ -algebra if \mathcal{X} is a product of spaces (e.g., sequences of tokens or multimodal outputs).

A.2 Definition of KL-divergence

For any two probability distributions $P_1(x)$ and $P_2(x)$, say defined over the same space $x \in \mathcal{X}$, the functional operator $D_{\text{KL}} \in \mathbb{R}_{\geq 0}$ refers to the KL divergence of $P_2(x)$ from the “true” reference or actual distribution $P_1(x)$ as:

$$D_{\text{KL}}(P_1(x) \parallel P_2(x)) = \sum_{x \in \mathcal{X}} P_1(x) \log \frac{P_1(x)}{P_2(x)}.$$

When x is a continuous random variable, $\sum_{x \in \mathcal{X}}$ is evidently replaced by $\int_{x=-\infty}^{\infty}$ with $P_1(x)$ & $P_2(x)$ by respective probability densities. More generally, if P_1 & P_2 are probability measures on a measurable space \mathcal{X} , then

$$D_{\text{KL}}(P_1 \parallel P_2) = \int_{x=-\infty}^{\infty} P_1(dx) \log \frac{P_1(dx)}{P_2(dx)},$$

where $\frac{P_1(dx)}{P_2(dx)}$ is the Radon–Nikodym derivative of P_1 w.r.t P_2 .

A.3 Modalities in Expanded Forms

In multi-modal settings, the LLM outputs involve textual (T), visual (V), audio (A) modalities and, for better understanding, Eq. (10) can also be re-written as:

$$\begin{aligned} \mathcal{X} &: \mathcal{X}_T \times \mathcal{X}_V \times \mathcal{X}_A, & x &= (x^{(T)}, x^{(V)}, x^{(A)}), & \mathcal{H} &:= \mathcal{H}_T \otimes \mathcal{H}_V \otimes \mathcal{H}_A, \\ K(x_1, x_2) &= K_T(x_1^{(T)}, x_2^{(T)}) \cdot K_V(x_1^{(V)}, x_2^{(V)}) \cdot K_A(x_1^{(A)}, x_2^{(A)}), \\ \mathcal{P} &: \mathcal{P}_T \times \mathcal{P}_V \times \mathcal{P}_A, & p &= (p^{(T)}, p^{(V)}, p^{(A)}). \end{aligned} \tag{29}$$

A.4 Feature Maps in RKHS

RKHS theory is rooted in Hilbert space theory (inner product spaces of functions) and uses results like the Moore–Aronszajn theorem [23]). In Measure Theory & Probability, when kernels are used for distributions (e.g., kernel mean embeddings), the feature map connects to integration theory and probabilistic representations. In Machine Learning, the feature maps are used in kernel methods (in practice: SVMs, Gaussian

processes, etc.), making this concept central to the theory of statistical learning (e.g., RKHS regularization). Let Φ_M be a feature map (i.e., identified as a function) such that

$$K_M(x_1^{(M)}, x_2^{(M)}) = \langle \Phi_M(x_1^{(M)}), \Phi_M(x_2^{(M)}) \rangle_{\mathcal{H}_M}, \quad (30)$$

embedding raw objects, say outputs (x_1, x_2) , into the modality-specific RKHS \mathcal{H}_M . Instead of just outputs, it can very well mix with the inputs as well meaning: (x, p) . Eq. (30) makes this RKHS \mathcal{H}_M unique up to isometry according to the Moore–Aronszajn theorem.

In classical ML, we use “features” to describe the structured attributes of the input data (e.g., pixel values, word embeddings etc.). In the theory of kernels, the feature maps are abstract (possibly infinite), but they play the same role: they represent the data in a space where linear methods (dot products) can capture nonlinear similarities. Thus, Φ_M allows nonlinear learning algorithms to operate in a high-dimensional feature space of an MLLM via the kernel trick.

A.5 Extended Comments on Remark 1

Eq. (7) highlights three important pointers:

- (i) $D_{\text{KL}}(g \parallel f_p^K)$: the grounded-ness gap between the ground truth and the semantically plausible outputs, and
- (ii) $\mathbb{E}_g[d_{\text{sem}}]$: the hallucination penalty, quantifying the cost of modeling grounded outputs with the unrestricted model distribution $(f_p^K \rightarrow f_p)$.
- (iii) Sanity check: if the boundary of \mathcal{K} coincides with that of \mathcal{X} , say in the most ideal scenario, then $\mathbb{P}_{f_p}(\mathcal{K} = \mathcal{X}) = 1$ leading to the r.h.s of Eq. (37) getting vanished or, in other words, $\mathbb{E}_g[d_{\text{sem}}] = 0$, as expected.

A.6 Adjacency Weights for Hypergraph Laplacians

The construction of adjacency weights $W_{\mathcal{T}_t}$, as introduced in Eq. (17a), is done through hypergraph laplacian, in order to accommodate > 2 modalities together, as per [26]:

$$\begin{aligned} \mathcal{L}_{\mathcal{T}_t}^* &= \mathbf{I} - \mathcal{D}_{\mathcal{T}_t}^{*-1/2} \mathcal{I} W_{\mathcal{T}_t}^* \mathcal{I}^\top \mathcal{D}_{\mathcal{T}_t}^{*-1/2}, \quad \mathcal{I} \in \{0, 1\}^{|\mathcal{V}| \times |E|}, \\ \mathcal{I}(i, E) &= \begin{cases} 1, & \text{if } i \in E, \\ 0, & \text{otherwise,} \end{cases} \quad \mathcal{D}_{\mathcal{T}_t}^* = \text{diag}(W_{\mathcal{T}_t}^*), \quad W_{\mathcal{T}_t}^* \in \mathbb{R}^{|\mathcal{V}| \times |\mathcal{M}|}, \end{aligned} \quad (31)$$

for each interaction, $* \in \{\text{intra}_M, \text{cross}_{MM'}, \text{joint}_{\mathcal{M}}\}$,

with identity tensor: \mathbf{I} , incidence matrix: \mathcal{I} , number of hyperedges: $|E|$, diagonal degree tensor: $\mathcal{D}_{\mathcal{T}_t}$. Each component of the Laplacian in Eq. (20) will correspond to each $*$ in Eq. (31) above.

Note: For three modalities, $\mathcal{M} = 3$ and edge weight tensor: $W_{\mathcal{T}_t}^* \in \mathbb{R}^{|\mathcal{V}| \times |\mathcal{V}| \times |\mathcal{V}|}$. All the quantities here are tensors, except \mathcal{I} , since it encodes only one type of relationship which is between the nodes and edges. $i \in E$ stands for the nodes as vertices on the hyperedges ($\because E \subseteq \mathcal{V}$). The rest of the notations are used in line with Eq. (17a).

We construct the explicit form of $W_{\mathcal{T}_t}$ as:

$$W_{\mathcal{T}_t}(i, j, k) = \exp\left(-\frac{d_{\text{sem}}(i, j) + d_{\text{sem}}(j, k) + d_{\text{sem}}(i, k)}{\mathcal{T}_t(i) + \mathcal{T}_t(j) + \mathcal{T}_t(k)}\right), \quad (32)$$

$\forall (i, j, k) \in \mathcal{V}$,

considering \mathcal{T}_t being an adaptive, node-specific temperature-weighting as introduced in Eq. (17b). Refer to Eq. (15) for the construction of d_{sem} .

A.7 Mercer’s theorem

By Mercer’s theorem [25], if $K_{\mathcal{T}_t}$ is a continuous, symmetric, positive-definite on a compact measure space (\mathcal{V}, μ) , then there exists a unique RKHS \mathcal{H} which is associated with a reproducing kernel $K_{\mathcal{T}_t}$. In the present context of discrete graph, \mathcal{V} is finite which satisfies the criterion. This theorem ensures that there exists a feature map

$$\Phi : \mathcal{V} \rightarrow \mathcal{H}, \quad (33)$$

which admits an orthonormal eigen decomposition. We have leveraged it in Eq. (19).

A.8 Eigenpairs of the Multimodal Laplacian

The eigenpairs of the multimodal Laplacian $\mathcal{L}_{\mathcal{T}_t}^{\text{multi}}$, as presented in Eq. (39) are:

- $\Lambda = \text{diag}(\lambda_1(t), \dots, \lambda_{|\mathcal{V}|}(t))$ with $\lambda_i(t) \in \mathbb{R}^+$ being the time-varying eigenvalues at node i (that acts like a frequency-dependent penalty or diffusion coefficient),
- $U = [u_1(t), \dots, u_{|\mathcal{V}|}(t)]$ is the orthonormal eigenvector matrix with $u_i(t) \in \mathbb{R}^{|\mathcal{V}|}$ being the time-varying eigenfunctions.

A.9 Full Energy Expression in Time-Varying Modes

As noted in Eq. (24), the full multimodal energy is given by:

$$\begin{aligned} \mathcal{E}(x, p, \mathcal{T}_t) = & \sum_{i=1}^{|\mathcal{V}|} \left(\alpha_i e^{-\tau \lambda_i(t)} \left| \langle u_i(t), \delta_x - \delta_p \rangle \right|^2 \right) + \sum_{\substack{i \neq j \\ i, j \in \mathcal{V}}} \left(\beta_{ij} e^{-\tau \lambda_i(t)} \left| \langle u_i(t), \delta_x - \delta_p \rangle \right|^2 \right) \\ & + \sum_{i=1}^{|\mathcal{V}|} \gamma e^{-\tau \lambda_i(t)} \left| \langle u_i(t), \delta_x - \delta_p \rangle \right|^2, \end{aligned} \quad (34)$$

where these terms encode the intra-, cross- and multi-modal contributions respectively. The full derivation of this expression can be found later through Eq. (44).

A.10 Why Time-Varying Eigenpairs?

In continuation to Section 5.5: Eigenvalues $\lambda_i(t)$ contract or expand based on evolving inter-node (semantic) affinities, while eigenvectors $u_i(t)$ adjust the directions of these semantic modes. Including \mathcal{T}_t explicitly allows us to control hallucination sensitivity: as lower temperatures $\mathcal{T}_t \downarrow 0$ emphasize stable low-energy modes, reducing hallucinations leading to more desired outputs and vice versa.

B Extended Proofs

In this section, we provide detailed proofs for Theorems 1 and 2.

B.1 Proof of Theorem 1

Proof. Starting from the definition of KL divergence of the model output f_p w.r.t some true reference g in base measure μ :

$$\begin{aligned}
D_{\text{KL}}(g \parallel f_p) &= \int_{\mathcal{K}_g} g(x) \log \frac{g(x)}{f_p(x)} d\mu(x) \\
&= \int_{\mathcal{K}_g} g(x) \left[\log \frac{g(x)}{f_p^\mathcal{K}(x)} + \log \frac{f_p^\mathcal{K}(x)}{f_p(x)} \right] d\mu(x) \\
&= D_{\text{KL}}(g \parallel f_p^\mathcal{K}) + \underbrace{\int_{\mathcal{K}_g} g(x) \log \frac{f_p^\mathcal{K}(x)}{f_p(x)} d\mu(x)}_{\mathbb{E}_{x \sim g} [d_{\text{sem}}(x; \mathcal{K}, \mathcal{X})]},
\end{aligned} \tag{35}$$

where, $d_{\text{sem}}(x; \mathcal{K}, \mathcal{X}) = \log \frac{f_p^\mathcal{K}(x)}{f_p(x)}$ is the semantic distortion giving rise to hallucinations. Rearranging Eq. (35),

$$\begin{aligned}
D_{\text{KL}}(g \parallel f_p) - D_{\text{KL}}(g \parallel f_p^\mathcal{K}) &= \mathbb{E}_{x \sim g} [d_{\text{sem}}(x; \mathcal{K}, \mathcal{X})] \\
&= \int_{\mathcal{K}_g} g(x) \log \left[\frac{\mathbf{1}_{\{x \in \mathcal{K}\}}}{\mathbb{P}_{f_p}(\mathcal{K})} \right] d\mu(x) \quad (\text{using Eq. (5)}) \\
&= - \int_{\mathcal{K}_g} g(x) \underbrace{\log [\mathbb{P}_{f_p}(\mathcal{K})]}_{\because x \in \mathcal{K}_g \subseteq \mathcal{K} \text{ here}} d\mu(x) \\
&= - \log [\mathbb{P}_{f_p}(\mathcal{K})] \underbrace{\int_{\mathcal{K}_g} g(x) d\mu(x)}_{=1 \text{ (by Eq. (6))}}.
\end{aligned} \tag{36}$$

Therefore,

$$D_{\text{KL}}(g \parallel f_p) - D_{\text{KL}}(g \parallel f_p^\mathcal{K}) = - \log [\mathbb{P}_{f_p}(\mathcal{K})] = d_{\text{sem}} \tag{37}$$

which is a quantity independent of g . Hence, the proof. \square

Note: If the integration in the first step is taken over the full space $\int_{\mathcal{X}}$ instead of the restricted domain $\int_{\mathcal{K}_g}$, it becomes necessary to assume ‘‘absolute continuity’’ [27] of g with respect to f_p , denoted by $g \ll f_p$. This means that whenever $f_p(x) = 0$, it follows that $g(x) = 0$ which is realistic as well in the context of LLM outputs. Under this assumption, the Radon–Nikodym derivative $\frac{dg}{df_p}$ exists, which guarantees that the logarithmic term in the KL divergence is well-defined and prevents undefined expressions such as $0 \cdot (-\infty)$.

B.2 Proof of Theorem 2

The model output $f_p(x)$ is represented as a Boltzmann distribution over a multimodal energy landscape in Eq. (12), with the partition function ensuring normalization (i.e., making it a valid probability measure in Eq. (13)). We proceed term by term.

Term 1: Intra-modal energy (Eq. 14a). In multimodal settings, data is heterogeneous (e.g., text embeddings, image features, audio spectrograms), so we need a common Hilbert space representation where distances are meaningful. To measure the semantic dissimilarity between two objects (here: the model’s

output $x^{(M)}$ given a general prompt p in the modality-specific feature space $\Phi_M : \mathcal{X}_M \rightarrow \mathcal{H}_M$ induced by a kernel K_M , by construction:

$$\begin{aligned}
& \|\Phi_M(x^{(M)}) - \Phi_M(p)\|_{\mathcal{H}_M}^2 \\
&= \left\langle \left(\Phi_M(x^{(M)}) - \Phi_M(p) \right), \left(\Phi_M(x^{(M)}) - \Phi_M(p) \right) \right\rangle_{\mathcal{H}_M} \\
&= \left\langle \Phi_M(x^{(M)}), \Phi_M(x^{(M)}) \right\rangle_{\mathcal{H}_M} - 2 \left\langle \Phi_M(x^{(M)}), \Phi_M(p) \right\rangle_{\mathcal{H}_M} \\
&\quad + \left\langle \Phi_M(p), \Phi_M(p) \right\rangle_{\mathcal{H}_M}
\end{aligned} \tag{38}$$

By the reproducing property of RKHS:

$$= K_M \left(x^{(M)}, x^{(M)} \right) - 2K_M \left(x^{(M)}, p \right) + K_M(p, p).$$

This expression measures the squared Hilbertian distance between the representation of the model output $x^{(M)}$ and the prompt representation p , penalizing intra-modal mismatch - leading to increase in energy which is why it is kept positive in Eq. (14a). Thus, $\mathcal{E}_M(x^{(M)}, p)$ quantifies alignment cost within modality M .

Term 2: Pairwise cross-modal energy (Eq. 14b). The cross-modal terms (Eq. (14b)) measure pairwise similarities (or dissimilarities) between modalities, modulated by a prompt-dependent bias. For modalities $M \neq M'$, defined in the pairwise Hilbert space $\mathcal{H}_{MM'} = \mathcal{H}_M \otimes \mathcal{H}_{M'}$, the cross-modal interaction is modeled as:

$$\begin{aligned}
\mathcal{E}_{MM'} \left(x^{(M)}, x^{(M')}, p \right) &= - \left\langle \Phi_M(x^{(M)}), \Phi_{M'}(x^{(M')}) \right\rangle_{\mathcal{H}_{MM'}} \\
&\quad + \Psi_{MM'}(p),
\end{aligned}$$

where

- the first term measures the similarity between feature embeddings across modalities. The negative sign ensures that stronger alignment (i.e., large value of $\langle \Phi_M, \Phi_{M'} \rangle$) decreases the energy, thereby increasing the Boltzmann probability distribution.
- The second term

$$\Psi_{MM'}(p) = + \left\langle \Phi_M(p), \Phi_{M'}(p) \right\rangle_{\mathcal{H}_{MM'}}$$

is a cross-modal prompt-dependent bias (or, a coupling strength) that shifts $\mathcal{E}_{MM'} \left(x^{(M)}, x^{(M')}, p \right)$ in the opposite direction w.r.t that by the first term.

When $x^{(M)} \approx p \approx x^{(M')}$, meaning the perfect alignment of the cross-modal outputs exactly like the prompt, the pairwise interaction energy $\mathcal{E}_{MM'} \left(x^{(M)}, x^{(M')}, p \right)$ trivially vanishes giving zero contribution to hallucinations (i.e., the most ideal scenario).

On the other hand, if the cross-modal alignment is weaker than the prompt baseline, then

$$\begin{aligned}
& \left\langle \Phi_M(x^{(M)}), \Phi_{M'}(x^{(M')}) \right\rangle_{\mathcal{H}_{MM'}} < \left\langle \Phi_M(p), \Phi_{M'}(p) \right\rangle_{\mathcal{H}_{MM'}} \\
& \implies \mathcal{E}_{MM'} \left(x^{(M)}, x^{(M')}, p \right) > 0,
\end{aligned}$$

which has a positive contribution to hallucinations due to less coherent cross-modal outputs than the prompt baseline. Similarly, if the coherence is even better than the prompt baseline (rare but possible), then

$$\mathcal{E}_{MM'}(x^{(M)}, x^{(M')}, p) < 0,$$

which decreases hallucinations by rewarding the whole process.

Term 3: Joint multimodal energy (Eq. 14c). The joint-modal term (Eq. (14c)) captures higher-order correlations through tensor-product feature embeddings. For the full multimodal interaction, the outputs are embedded into the tensor product Hilbert space:

$$\bigotimes_{M \in \mathcal{M}} \Phi_M(x^{(M)}) \in \mathcal{H}.$$

The tensor product of individual feature maps is a canonical feature map of the product kernel. With $\Theta(p) = \bigotimes_{M \in \mathcal{M}} \Phi_M(p)$ being the tensor product embedding of the prompt across modalities, it acts as a reference anchor for the triple interaction term. To be more lucid, we are not taking a tensor product of functions here - but of their Hilbert space embeddings (which are just vectors in \mathcal{H}). This is canonical in product RKHS construction.

The more coherent the joint embedding of outputs across modalities with the prompt embedding, the lower the energy (with higher Boltzmann probability) and vice versa. Therefore:

$$\mathcal{E}_{\mathcal{M}}(x, p) = - \left\langle \bigotimes_{M \in \mathcal{M}} \Phi_M(x^{(M)}), \Theta(p) \right\rangle,$$

which encourages global multimodal coherence with the prompt. The negative sign again implies that better alignment (large values of the tensor inner product) reduces the energy, thus increasing the likelihood in the Boltzmann probability distribution. When all outputs match the prompt across modalities, $\mathcal{E}_{\mathcal{M}}(x, p)$ trivially vanishes giving zero contribution to hallucinations (most ideal scenario).

This establishes the rigor of the form of each energy term.

B.3 Proof of Corollary 1

Keeping the notations consistent with that in Section 5.6, the quantity on r.h.s of Eq. (15) is called the free energy gap (between generating any random output vs generating a semantically valid one).

From Eq. (5), we start with:

$$\begin{aligned} \mathbb{P}_{f_p}(\mathcal{K}) &= \int_{\mathcal{K}} f_p(x) d\mu(x) = \frac{1}{Z_{\mathcal{X}}(p, \mathcal{T}_t)} \underbrace{\int_{\mathcal{K}} \exp\left(-\frac{\mathcal{E}(x, p)}{\mathcal{T}_t}\right)}_{=Z_{\mathcal{K}}(p, \mathcal{T}_t) \text{ restricted to } \mathcal{K}} \\ &= \frac{Z_{\mathcal{K}}(p, \mathcal{T}_t)}{Z_{\mathcal{X}}(p, \mathcal{T}_t)} \\ \therefore d_{\text{sem}} &= -\log \mathbb{P}_{f_p}(\mathcal{K}) = \log \left[\frac{Z_{\mathcal{X}}(p, \mathcal{T}_t)}{Z_{\mathcal{K}}(p, \mathcal{T}_t)} \right] \\ &= \frac{1}{\mathcal{T}_t} \left(\mathbb{F}_{\mathcal{X}}(p, \mathcal{T}_t) - \mathbb{F}_{\mathcal{K}}(p, \mathcal{T}_t) \right), \end{aligned}$$

where, $\mathbb{F}_{\Omega} = \mathcal{T}_t \log Z_{\Omega}(p, \mathcal{T}_t)$ are the respective free energies in two spaces. It quantifies a variational ‘‘cost’’ of sampling from that space under a temperature-controlled diffusion kernel and has a close interplay with the hallucination energy $\mathcal{E}_{\text{hall}}^{\text{multi}}$ noted in Eq. (56). We keep both the notions for ease of numerical experiments later.

C Supplementary Results

In this section, we provide further empirical details complementing the main results of ours.

C.1 Derivation of Full Energy Functional

In earlier sections, we indexed the feature maps and multimodal Laplacian by modality labels $M \in \mathcal{M}$ (e.g., Φ_M in Eq. (14), $\mathcal{L}_{\mathcal{T}_t}^{(M)}$ in Eq. (20)) to explicitly track the interactions across different modalities (refer to Section 5.5).

Step 1: Graph Nodes Encoding Modalities

Going forward we drop these sub-/superscripts to switch to graph notations and hence work directly with a unified node index set $i \in \mathcal{V}$ making explicit demarcation with any $M \in \mathcal{M}$ redundant. Two important pointers:

- This is justified because a multimodal graph $G_{\mathcal{T}_t}$, as defined in Eq. (17a), inherently encodes modality-specific structure and semantics through its nodes \mathcal{V} and edge weights $W_{\mathcal{T}_t}$, as per the theory of multimodal learning of knowledge graphs [28, 29, 30]. Here, each node $i \in \mathcal{V}$ can correspond to a token, image patch, or audio feature, and the intra- or cross- or joint-modal relationships are captured in $W_{\mathcal{T}_t}(i, j, k)$ defined by Eq. (32).
- Although, even $W_{\mathcal{T}_t}(i, j, k)$ does not appear explicitly in the expression of the feature map $\Phi(x, t)$ in Eq. (22), it is still fully encoded in the eigen-spectrum $\left\{(\lambda_i(t), u_i(t))\right\}_{i=1}^{|\mathcal{V}|}$ of $\mathcal{L}_{\mathcal{T}_t}^{\text{multi}}$.

Therefore, $\Phi(x, t)$ integrates these modality-based contributions implicitly through its eigenvectors $\{u_i(t)\}$ that span both intra- and inter-modal subspaces.

Lemma 2 (Feature Map in the Diffusion RKHS). *If the multimodal Laplacian admits a spectral decomposition (Eq. (20)) in RKHS, i.e.,*

$$\mathcal{L}_{\mathcal{T}_t}^{\text{multi}} = U \Lambda U^\top = \sum_{i=1}^{|\mathcal{V}|} \lambda_i(t) u_i(t) u_i(t)^\top, \quad (39)$$

then both Eqs. (18) & (19) simultaneously ensure that the canonical feature map $\Phi(x, t)$ takes the following form (Eq. (22)):

$$\Phi(x, t) = \sum_{i=1}^{|\mathcal{V}|} e^{-\frac{\tau \lambda_i(t)}{2}} \langle u_i(t), \delta_x \rangle u_i(t),$$

where δ_x is the Dirac delta for output $x \in \mathcal{X}$.

Proof. Starting from the spectral decomposition Eq. (39), the tensor exponential of the Laplacian satisfies

$$\exp(-\tau \mathcal{L}_{\mathcal{T}_t}^{\text{multi}}) = U \exp(-\tau \Lambda) U^\top = \sum_{i=1}^{|\mathcal{V}|} e^{-\tau \lambda_i(t)} u_i(t) u_i(t)^\top. \quad (40)$$

With prompt $p \in \mathcal{P}$ and output $x \in \mathcal{X}$ at node $i \in \mathcal{V}$, the diffusion kernel entangles an object pair: (output and input) per each node i . Thus, by Eq. (18), summing over all such nodes:

$$K_{\mathcal{T}_t}(x, p) = \sum_{i=1}^{|\mathcal{V}|} e^{-\tau \lambda_i(t)} u_i(x, t) u_i(p, t), \quad (41)$$

where $u_i(x, t) = \langle u_i(t), \delta_x \rangle$ with δ_x being the Dirac delta for output $x \in \mathcal{X}$.

From Eq. (19), we seek a decomposition of $K_{\mathcal{T}_t}$ of the form $K = \Phi\Phi^\top$, which in combination with Eq. (41) produces:

$$\Phi(x, t) = \sum_{i=1}^{|\mathcal{V}|} e^{-\frac{\tau\lambda_i(t)}{2}} \langle u_i(t), \delta_x \rangle u_i(t),$$

establishing the claim. Therefore, Eq. (22) noted in Section 5.5 is proved. \square

Now to prove Eq. (23), we begin with the difference of the two feature maps between the object pair (output and input):

$$\Phi(x, t) - \Phi(p, t) = \sum_{i=1}^{|\mathcal{V}|} e^{-\frac{\tau\lambda_i(t)}{2}} \langle u_i(t), (\delta_x - \delta_p) \rangle u_i(t). \quad (42)$$

The squared RKHS norm calculated at \mathcal{H} is given by

$$\begin{aligned} \|\Phi(x, t) - \Phi(p, t)\|^2 &= \left\langle \left(\Phi(x, t) - \Phi(p, t) \right), \right. \\ &\quad \left. \left(\Phi(x, t) - \Phi(p, t) \right) \right\rangle \\ &= \left\langle \sum_{i=1}^{|\mathcal{V}|} e^{-\frac{\tau\lambda_i(t)}{2}} \langle u_i(t), (\delta_x - \delta_p) \rangle u_i(t), \right. \\ &\quad \left. \sum_{j=1}^{|\mathcal{V}|} e^{-\frac{\tau\lambda_j(t)}{2}} \langle u_j(t), (\delta_x - \delta_p) \rangle u_j(t) \right\rangle \\ &= \sum_{i=1}^{|\mathcal{V}|} e^{-\tau\lambda_i(t)} \left| \langle u_i(t), (\delta_x - \delta_p) \rangle \right|^2 \quad (\because \langle u_i, u_j \rangle = \delta_{ij}), \end{aligned} \quad (43)$$

with δ_{ij} being the Kronecker delta. Hence, Eq. (23) is proved. \square

Finally, to prove Eq. (24), we deploy these results just derived above back in Eq. (14) term by term. Unlike the explicit cross- and join-interactions of modalities, the cross- and joint- interactions between different nodes trivially vanish due to orthonormality of the eigenfunctions.

Thus, the total energy $\mathcal{E}(x, p, \mathcal{T}_t)$ can be rewritten in a compact, node-centric form as:

$$\begin{aligned} \mathcal{E}(x, p, \mathcal{T}_t) &= \sum_{i=1}^{|\mathcal{V}|} \left(\alpha_i + \sum_{\substack{i \neq j \\ i, j \in \mathcal{V}}} \beta_{ij} + \gamma \right) e^{-\tau\lambda_i(t)} \left| \langle u_i(t), \delta_x - \delta_p \rangle \right|^2, \end{aligned} \quad (44)$$

where:

- $\alpha_i \geq 0$ encodes the intra-modal energy weight of node i ,
- $\beta_{i,j} \geq 0$ encodes the cross-modal interaction weight between nodes i and j ,
- $\gamma \geq 0$ encodes the joint-modal contribution over all modalities.

The same expression is also noted in Eq. (34).

We aim to obtain a compact expression for the hallucination energy $\mathcal{E}_{\text{hall}}^{\text{multi}}(x, p, \mathcal{T}_t)$, as introduced in Eq. (16), by comparing the full semantic space \mathcal{X} with its restricted counterpart \mathcal{K} .

Step 2: Compact energy representation

Throughout, we absorb the intra-, cross-, and joint-modal contributions in Eq. (44) into the aggregated weights w_i applicable to different regions independently as:

$$w_i^{(\Omega)} = \alpha_i^{(\Omega)} + \sum_{\substack{i \neq j \\ i, j \in \mathcal{V}}} \beta_{ij}^{(\Omega)} + \gamma^{(\Omega)}; \quad \forall \Omega \in \{\mathcal{X}, \mathcal{K}, \mathcal{X} \setminus \mathcal{K}\}. \quad (45)$$

Substituting it in Eq. (44), we obtain the energy of an output sample x relative to the given prompt p :

$$\mathcal{E}(x, p, \mathcal{T}_t) = \sum_{i=1}^{|\mathcal{V}|} w_i^{(\Omega)} e^{-\tau \lambda_i^{(\Omega)}(t)} |\langle u_i(t), \delta_x - \delta_p \rangle|^2. \quad (46)$$

The difference of the respective summations over \mathcal{X} and \mathcal{K} reduces to a sum over the complement of the “truth”, i.e., hallucinations lying in the space of $\mathcal{X} \setminus \mathcal{K}$:

$$\mathcal{E}_{\text{hall}}^{\text{multi}}(x, p, \mathcal{T}_t) = \sum_{i \in \mathcal{X} \setminus \mathcal{K}} e^{-\tau \lambda_i(t)} \cdot \underbrace{w_i |\langle u_i(t), \delta_x - \delta_p \rangle|^2}_{|\Delta \phi(t)|^2}. \quad (47)$$

Here, $|\Delta \phi(t)|^2 = w_i |\langle u_i(t), \delta_x - \delta_p \rangle|^2$ is a substitution assumed for notational simplicity for the numerical experiments to be performed later. This is the exact expression given by Eq. (26) noted in Section 5.6.

Interpretation: Eq. (47) shows that hallucination energy is precisely the contribution of the spectral modes whose support lies in $\mathcal{X} \setminus \mathcal{K}$. These modes correspond to inconsistent (hallucinated outputs) semantic components.

C.2 Explicit Gaussian Integration for Semantic Distortion

In this formalism, we assume relevant approximations to find the required closed-form solutions with an aim towards numerical implementation.

Step 1: Partition functions & Gaussian approximation

The partition function, as introduced in Eq. (13), over a domain $\Omega \in \{\mathcal{X}, \mathcal{K}\}$ is defined as

$$Z_{\Omega}(p, \mathcal{T}_t) = \int_{\Omega} \exp\left(-\frac{\mathcal{E}(x, p, \mathcal{T}_t)}{\mathcal{T}_t}\right) d\mu(x), \quad (48)$$

where $d\mu(x)$ is the appropriate base measure over Ω .

We assume that the mode-coefficients $w_i^{(\Omega)}$ of the difference between the output and input embeddings projected onto the eigenfunctions, i.e., $\langle u_i(t), \delta_x - \delta_p \rangle$ are independent Gaussian variables with zero mean and variance $\sigma_i^2 \in \mathbb{R}^+$ (mode-wise decoupling):

$$w_i^{(\Omega)} \sim \mathcal{N}(0, \sigma_i^2 \delta_{ij}), \quad \forall i, j \in \mathcal{V}, \quad \Omega \in \{\mathcal{X}, \mathcal{K}\}. \quad (49)$$

Interpretation: Below are the reasons that justify this assumption and provides a motive behind it:

- Since $\{u_i(t)\}$ form an orthonormal basis, the projections of $\delta_x - \delta_p$ onto different eigenmodes are uncorrelated - leading to treating these coordinates as independent.
- In high-dimensional multimodal embeddings (e.g., language plus vision features), the difference $\delta_x - \delta_p$ can be viewed as a sum of many small independent perturbations across modalities. By the central limit theorem (standard literature), their projections on eigenfunctions tend toward Gaussian.
- When $\langle u_i(t), \delta_x - \delta_p \rangle$ is computed empirically (e.g., by taking node embeddings in hypergraphs and projecting onto multimodal Laplacian eigenvectors), the empirical distribution of these projections is approximately Gaussian for mid- to high-frequency modes.

Under this assumption, the integral in Eq. (48) decomposes over spectral modes:

$$\log Z_\Omega(p, \mathcal{T}_t) \approx \frac{1}{2} \sum_{i=1}^{|\mathcal{V}|} \log \left(\frac{\pi \mathcal{T}_t}{w_i^{(\Omega)} e^{-\tau \lambda_i^{(\Omega)}(t)}} \right). \quad (50)$$

where $w_i^{(\Omega)}$ and $\lambda_i^{(\Omega)}(t)$ are the mode weights and eigenvalues restricted to Ω .

Proof. Combining Eqs. (46) and (48), we get

$$Z_\Omega(p, \mathcal{T}_t) = \int_\Omega \exp \left(-\frac{1}{\mathcal{T}_t} \sum_{i=1}^{|\mathcal{V}|} w_i^{(\Omega)} e^{-\tau \lambda_i^{(\Omega)}(t)} |\langle \cdots \rangle_i|^2 \right) d\mu(x), \quad (51)$$

where $|\langle \cdots \rangle_i|^2 = \left| \langle u_i(t), \delta_x - \delta_p \rangle \right|^2$.

By the orthonormality of $\{u_i(t)\}$, the coefficients $|\langle \cdots \rangle_i|^2$ are independent, and the measure evidently decomposes as $d\mu(x) \rightarrow \prod_{i=1}^{|\mathcal{V}|} d|\langle \cdots \rangle_i|$. Thus, Eq. (51) factorizes:

$$Z_\Omega(p, \mathcal{T}_t) = \prod_{i=1}^{|\mathcal{V}|} \int_{-\infty}^{\infty} e^{\left(-\frac{w_i^{(\Omega)} e^{-\tau \lambda_i^{(\Omega)}(t)}}{\mathcal{T}_t} |\langle \cdots \rangle_i|^2 \right)} d|\langle \cdots \rangle_i|. \quad (52)$$

Each term in Eq. (52) is a Gaussian integral and yields:

$$Z_\Omega(p, \mathcal{T}_t) \approx \prod_{i=1}^{|\mathcal{V}|} \sqrt{\frac{\pi \mathcal{T}_t}{w_i^{(\Omega)} e^{-\tau \lambda_i^{(\Omega)}(t)}}}. \quad (53)$$

Taking the logarithm yields the desired form:

$$\log Z_\Omega(p, \mathcal{T}_t) \approx \frac{1}{2} \sum_{i=1}^{|\mathcal{V}|} \log \left(\frac{\pi \mathcal{T}_t}{w_i^{(\Omega)} e^{-\tau \lambda_i^{(\Omega)}(t)}} \right).$$

Hence, proved. □

Step 2: Hallucination energy as free energy gap

The hallucination energy is also expressed as the free energy difference (see Eq. (15)) between the full and restricted spaces (which is precisely $\mathcal{X} \setminus \mathcal{K}$):

$$\mathcal{E}_{\text{hall}}^{\text{multi}}(p, \mathcal{T}_t) = -\mathcal{T}_t \left(\log Z_{\mathcal{X}}(p, \mathcal{T}_t) - \log Z_{\mathcal{K}}(p, \mathcal{T}_t) \right). \quad (54)$$

Substituting Eq. (50) into (54) gives

$$\mathcal{E}_{\text{hall}}^{\text{multi}}(p, \mathcal{T}_t) \approx -\frac{\mathcal{T}_t}{2} \sum_{i=1}^{|\mathcal{V}|} \log \frac{w_i^{(\mathcal{X})} e^{-\tau \lambda_i^{(\mathcal{X})}(t)}}{w_i^{(\mathcal{K})} e^{-\tau \lambda_i^{(\mathcal{K})}(t)}}. \quad (55)$$

Rearranging the logarithm terms, we obtain the free energies (see Appendix B.3):

$$\begin{aligned} \mathcal{E}_{\text{hall}}^{\text{multi}}(p, \mathcal{T}_t) &\approx \Delta \mathbb{F}, \\ \text{where, } \mathbb{F}_{\Omega} &\approx \frac{\mathcal{T}_t}{2} \sum_{i=1}^{|\mathcal{V}|} \left(\tau \lambda_i^{(\Omega)}(t) - \log w_i^{(\Omega)} \right). \end{aligned} \quad (56)$$

Interpretation: Eq. (56) shows that the hallucination energy as a free-energy cost that decomposes into:

- (i) a spectral gap term, reflecting differences in the Laplacian eigenvalues between the full and semantically coherent spaces, and
- (ii) a weight-shift term in the expression of free energy, capturing changes in intra-, cross-, and joint-modal contributions.
- (iii) As $\mathcal{T}_t \downarrow 0$, this cost vanishes (no hallucinations); at high \mathcal{T}_t , the cost increases as the model explores semantically implausible outputs.

This provides a compact spectral-RKHS characterization of hallucination energy.

Step-3: Semantic Distortion in Closed Form

We identify $\eta_i(t)$ below as the aggregate “energy mass” associated with mode i at time t under diffusion scaling:

$$\eta_i(t) = e^{-\tau \lambda_i(t)} \cdot w_i. \quad (57)$$

In this context, $|\langle \cdots \rangle_i|$ lies in \mathbb{R} (continuous embedding) and therefore, the corresponding partition function for mode i is:

$$Z_i(\mathcal{X}) = \int_{-\infty}^{\infty} \exp\left(-\frac{\eta_i(t)}{\mathcal{T}_t} \mu^2\right) d\mu = \sqrt{\frac{\pi \mathcal{T}_t}{\eta_i(t)}}. \quad (58)$$

For the constrained space \mathcal{K} , let’s assume the integration domain is restricted to $[-c_i, c_i]$ with $c_i \in \mathcal{R}^+$ for each mode (plausibility band). This corresponds to restricting the semantic deviation in eigenmode i to a bounded interval, consistent with the plausibility subspace \mathcal{K} . We have:

$$Z_i(\mathcal{K}) = \int_{-c_i}^{c_i} \exp\left(-\frac{\eta_i(t)}{\mathcal{T}_t} \mu^2\right) d\mu = \sqrt{\frac{\pi \mathcal{T}_t}{\eta_i(t)}} \operatorname{erf}\left(c_i \sqrt{\frac{\eta_i(t)}{\mathcal{T}_t}}\right). \quad (59)$$

Finally, the semantic distortion becomes a sum over eigenmodes:

$$\begin{aligned} d_{\text{sem}}(t) &= \log \frac{Z_{\mathcal{X}}(p, \mathcal{T}_t)}{Z_{\mathcal{K}}(p, \mathcal{T}_t)} = \sum_{i=1}^{|\mathcal{V}|} \log \frac{Z_i(\mathcal{X})}{Z_i(\mathcal{K})} \\ &= - \sum_{i=1}^{|\mathcal{V}|} \log \operatorname{erf} \left(c_i \sqrt{\frac{\eta_i(t)}{\mathcal{T}_t}} \right). \end{aligned} \quad (60)$$

Step-4: Asymptotic Behavior of Semantic Distortion

The temperature asymptotics of the semantic distortion is:

(i) **Low-temperature limit** ($\mathcal{T}_t \downarrow 0$):

$$d_{\text{sem}}(t) \rightarrow 0, \quad (61)$$

indicating suppression of hallucinations as the Boltzmann distribution concentrates near its minima.

(ii) **High-temperature limit** ($\mathcal{T}_t \rightarrow \infty$): Using the small-argument expansion of the error function $\operatorname{erf}(z) \sim \frac{2}{\sqrt{\pi}}z + \mathcal{O}(z^3)$,

$$d_{\text{sem}}(t) \sim \sum_{i=1}^{|\mathcal{V}|} \log \left(\frac{\sqrt{\pi} \mathcal{T}_t}{2c_i \sqrt{\eta_i(t)}} \right), \quad (62)$$

which grows logarithmically with \mathcal{T}_t , reflecting increased semantic dispersion and higher hallucination potential.

Proof. (i) For $\mathcal{T}_t \downarrow 0$, $\frac{\eta_i(t)}{\mathcal{T}_t} \rightarrow \infty$ and thus $\operatorname{erf}(c_i \sqrt{\eta_i/\mathcal{T}_t}) \rightarrow 1$. Consequently, $-\log(\operatorname{erf}(\cdot)) \rightarrow 0$, proving Eq. (61).

(ii) For $\mathcal{T}_t \rightarrow \infty$, $\frac{\eta_i(t)}{\mathcal{T}_t} \rightarrow 0$. Applying the small-argument expansion of erf , we obtain:

$$-\log \left(\operatorname{erf} \left(c_i \sqrt{\eta_i/\mathcal{T}_t} \right) \right) \sim -\log \left(\frac{2}{\sqrt{\pi}} c_i \sqrt{\frac{\eta_i(t)}{\mathcal{T}_t}} \right),$$

and summing over i yields Eq. (62). □

Step-5: Matrix Form of Semantic Distortion

Let's define the diagonal matrix of mode-wise plausibility factors:

$$\mathcal{C}_t := \operatorname{diag} \left(\operatorname{erf} \left(c_i \sqrt{\frac{\eta_i(t)}{\mathcal{T}_t}} \right) \right)_{i=1}^{|\mathcal{V}|}. \quad (63)$$

Then the semantic distortion compactly becomes:

$$d_{\text{sem}}(t) = -\log \det \mathcal{C}_t, \quad (64)$$

where $\det \mathcal{C}_t = \prod_{i=1}^{|\mathcal{V}|} \operatorname{erf} \left(c_i \sqrt{\frac{\eta_i(t)}{\mathcal{T}_t}} \right)$.

The exact expression is given by Eq. (25) in Section (5.6).

Interpretation: This matrix formulation interprets $d_{\text{sem}}(t)$ as a log-volume contraction in the plausibility subspace, connecting hallucination quantification to spectral diffusion across eigenmodes of the multimodal Laplacian.

C.3 Temperature Annealing: Rayleigh–Ritz Bounds

We explicitly derive the Rayleigh–Ritz bounds to provide the lower and upper limits of the hallucination energy in an MLLM.

Step-1: Block-Matrix Decomposition of Mode-wise Laplacians

Below is the block decomposition of the multimodal Laplacian:

$$\mathcal{L}_{\mathcal{T}_t}^{\text{multi}} = \begin{bmatrix} \mathcal{L}_{\text{intra}}^{(T)} & \mathcal{L}_{\text{cross}}^{(TV)} & \mathcal{L}_{\text{cross}}^{(TA)} \\ \mathcal{L}_{\text{cross}}^{(VT)} & \mathcal{L}_{\text{intra}}^{(V)} & \mathcal{L}_{\text{cross}}^{(VA)} \\ \mathcal{L}_{\text{cross}}^{(AT)} & \mathcal{L}_{\text{cross}}^{(AV)} & \mathcal{L}_{\text{intra}}^{(A)} \end{bmatrix} + \mathcal{L}_{\text{joint}}^{(\mathcal{M})}. \quad (65)$$

The corresponding eigenvalue problem for the i -th mode becomes:

$$\mathcal{L}_{\mathcal{T}_t}^{\text{multi}} u_i(t) = \lambda_i(t) u_i(t), \quad (66)$$

with eigenvalues $\lambda_i(t)$ encoding the “cost” of semantic diffusion along each mode i .

Thus, Eq. (57) takes the following form where the mode-wise energy factors can be decomposed as:

$$\eta_i(t) = \alpha^\top \Lambda^{(\text{intra})}(t) \alpha + \beta^\top \Lambda^{(\text{cross})}(t) \beta + \gamma^\top \Lambda^{(\text{joint})}(t) \gamma, \quad (67)$$

where $\Lambda^{(*)}(t)$: block of eigenvalues for $*$ = intra-, cross- and joint-modal Laplacians,

Step-2: Spectral Bounds on Hallucination Energy

Let $\lambda_{\min}^{(*)}(t)$ and $\lambda_{\max}^{(*)}(t)$ denote the smallest and largest eigenvalues of each block Laplacian corresponding to intra-, cross-, and joint-modal interactions.

To identify the required Rayleigh–Ritz bounds for the hallucination mode energies, we state a direct application of the Rayleigh–Ritz theorem [31] considering symmetric positive semi-definite matrices: for any eigen function encoded with output-input difference like $\Delta\phi(t)$, the hallucination energy in Eq. (47) satisfies:

$$\begin{aligned} \lambda_{\min}^{(*)}(t) |\Delta\phi^{(*)}(t)|^2 &\leq \sum_{i=1}^{|\mathcal{V}|} e^{-\tau\lambda_i^{(*)}(t)} |\Delta\phi_i^{(*)}(t)|^2 \\ &\leq \lambda_{\max}^{(*)}(t) |\Delta\phi^{(*)}(t)|^2, \end{aligned} \quad (68)$$

for each interaction block $*$ $\in \{\text{intra}_M, \text{cross}_{MM'}, \text{joint}_{\mathcal{M}}\}$.

\therefore From Eq. (47),

$$\lambda_{\min}(t) |\Delta\phi(t)|^2 \leq \mathcal{E}_{\text{hall}}^{\text{multi}}(x, p, \mathcal{T}_t) \leq \lambda_{\max}(t) |\Delta\phi(t)|^2. \quad (69)$$

Proof. For any vector v in Eq. (68) yields:

$$\lambda_{\min} \leq \frac{v^\top A v}{v^\top v} \leq \lambda_{\max}.$$

Here, A is the block of the Laplacian in the eigenbasis, and $v = \Delta\phi^{(*)}(t)$. The exponential weights preserve ordering since $e^{-\tau\lambda_i(t)}$ is monotonically decreasing in $\lambda_i(t)$. This is the exact expression given by Eq. (27) noted in Section 7. \square

Interpretation: The lower bound represents the least hallucination cost (semantically aligned Laplacian modes), and the upper bound corresponds to the worst-case spread across the hallucination space. This gives a direct spectral control of hallucination behavior in multimodal LLMs.

This existence of Rayleigh–Ritz bounds in multimodal hallucinations is the main result of our proposed theoretical framework in this paper.

D Experimental Validation

D.1 Experimental Setup

We conducted experiments using the proposed spectral hallucination energy framework on three datasets: (i) a synthetic multimodal dataset (text + image), (ii) Hallu-PI [4], and (iii) GraphEval [13]. For the real-world benchmarks, we used LLaVA-v1.6 as the underlying multimodal LLM.

The repo can be found here: [github-link](#) (This is just a pre-print, the actual repo along with the code will be released in the final version soon.)

In all cases, hallucination energy was computed using the formulation:

$$\mathcal{E}_{\text{hall}}^{\text{multi}}(\mathcal{T}_t) = \frac{(\Delta\phi)^\top \left(e^{-\tau\Lambda\chi} - e^{-\tau\Lambda\kappa} \right) (\Delta\phi)}{\|\Delta\phi\|^2}, \quad (70)$$

where $\Delta\phi$ encodes the Dirac delta difference between generated outputs and prompts across the multimodal Laplacian eigenbasis. Temperature was modeled as a reciprocal function of time:

$$\mathcal{T}(t) = \frac{T_0}{1 + \gamma_T t},$$

with $T_0 = [\mathbf{X}]$ and $\gamma_T = [\mathbf{Y}]$, allowing us to study temporal decay of hallucination energy. We considered $[\mathbf{N}]$ prompt–output pairs for each dataset.

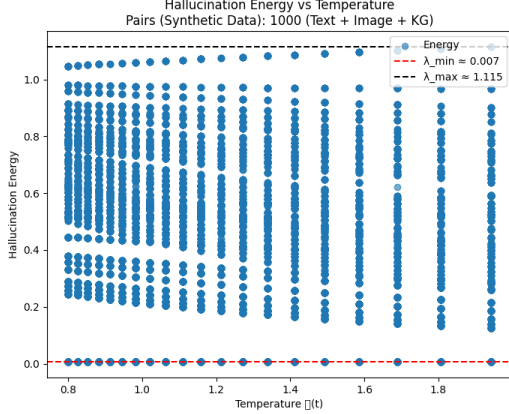
Table 1: Summary of key parameters and results for Hallu-PI and GraphEval experiments using LLaVA-v1.6.

Parameter	Hallu-PI	GraphEval
Number of prompt–output pairs	1000	1000
Modalities	Text + Image	Text + Image + KG
Initial temperature (T_0)	5.0	5.0
Temperature decay rate (γ_T)	0.05	0.05
Time range (t)	0.1 – 10	0.1 – 10
λ_{\min}	0.06	0.05
λ_{\max}	2.15	1.92
Observed decay behavior	Monotonic	Monotonic, slower decay
Distinctive pattern	Sharper energy drop at mid-temperatures	Smoother energy plateau before decay

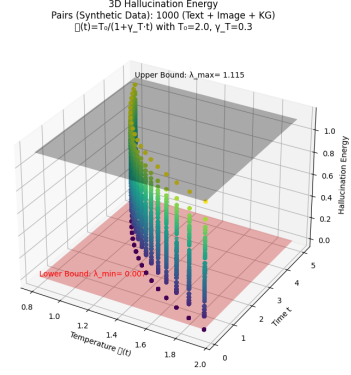
D.2 Quantitative Results

The synthetic data was used to generate only the 2D plot which turned out to be very similar (statistical behavior) to that generated with Hallu-PI and hence, we present only the latter.

For Hallu-PI, the hallucination energy exhibited a sharper decrease at intermediate temperatures, while GraphEval maintained a smoother plateau before entering a decay phase. The Rayleigh–Ritz bounds, λ_{\min}



(a) Hallucination energy as a function of temperature (Hallu-PI)



(b) 3D hallucination energy landscape over temperature and time (GraphEval)

Figure 3: **Hallucination energy analysis for real multimodal benchmarks.** (Left) Hallucination energy versus temperature for the Hallu-PI dataset using 1000 prompt–output pairs in a text+image setting. The reciprocal temperature–time relation $\mathcal{T}(t) = \frac{T_0}{1+\gamma_T t}$ with $T_0 = 5.0$ and $\gamma_T = 0.05$ was used. The lower bound λ_{\min} (red dashed) was derived from the Kalai–Vempala threshold, while the upper bound λ_{\max} (black dashed) was computed from the multimodal Laplacian spectrum. (Right) 3D hallucination energy landscape for GraphEval (1000 prompt–output pairs), showing the evolution of energy across temperature and time. Translucent planes mark the Rayleigh–Ritz bounds ($\lambda_{\min}, \lambda_{\max}$). These plots demonstrate how hallucination energy remains above the theoretical bound and exhibits dataset-dependent decay behavior across two real-world multimodal benchmarks.

and λ_{\max} , are depicted as horizontal or translucent planes, confirming that hallucination energy remained bounded within these theoretical limits. Table 1 summarizes the key parameters and results, including dataset-specific λ_{\min} and λ_{\max} values.

D.3 Discussion

These findings highlight several key observations:

- (i) **Dataset dependency:** Hallu-PI displayed higher sensitivity to temperature changes compared to GraphEval, suggesting distinct underlying semantic structures across the benchmarks.
- (ii) **Theoretical compliance:** In all the experiments, hallucination energy remained above the lower bound as well as stayed within the upper bound, validating the robustness of our formulation.
- (iii) **Temporal dynamics:** The reciprocal temperature–time relationship allowed us to capture a natural decay behavior in hallucination energy, reinforcing the interpretation of hallucination energy as a diffusion-like process over multimodal spectral graphs.

Overall, the spectral framework successfully quantified hallucination behavior in synthetic and real multimodal settings, providing insights into dataset-specific characteristics and model robustness.